ELSEVIER

Contents lists available at ScienceDirect

# International Journal of Thermal Sciences

journal homepage: www.elsevier.com/locate/ijts





# Experimental investigation on the uneven distribution characteristics of sCO<sub>2</sub> flow in vertically parallel double pipes with non-uniform heating

Wenxuan Cao<sup>a</sup>, Jinliang Xu<sup>a,b</sup>, Enhui Sun<sup>a,\*</sup>, Yaru Ma<sup>a</sup>

- a Beijing Key Laboratory of Multiphase Flow and Heat Transfer for Low Grade Energy Utilization, North China Electric Power University, Beijing, 102206, China
- b Key Laboratory of Power Station Energy Transfer Conversion and System, North China Electric Power University, Ministry of Education, Beijing, 102206, China

#### ARTICLE INFO

Keywords:
Parallel
Supercritical CO<sub>2</sub>
Thermal deviation
Flow distribution
Self compensation characteristics
Orifice contraction effects

#### ABSTRACT

Exploring the matching relationship between heat source heat and working fluid flow is crucial to improve boiler thermal efficiency and suppress superheating of heat exchanger walls. This paper takes the cooling wall of supercritical carbon dioxide (sCO<sub>2</sub>) boilers as the research object, and investigates the influence of inter-tube heat deviation  $\varphi$  on flow distribution characteristics. Specific experiments were conducted on parallel dual pipelines with an inner diameter of 10 mm for sCO<sub>2</sub> flow heat transfer, with a test pressure of 7.5 MPa~15 MPa, total mass flow rate  $G_{\rm all}$  of 600 kg/m²s~1400 kg/m²s, heat flux  $q_{\rm w}$  of 50 kW/m²~350 kW/m², and  $\varphi$  of 0.8~1.25. In this study, Bu number and Re number were used to characterize the promoting effect of shear force on vertical upward flow, while K number was used to characterize the hindering effect of evaporative momentum force on flow. The results show that, unlike the traditional flow distribution theory based on the same principle of total pressure drop in parallel tube branches, this new experimental correlation equation obtained from the perspective of force analysis has an average relative error, average absolute relative error, and root mean square relative error of -0.04%, 0.73%, and 0.90%, respectively. It can more accurately predict the flow distribution characteristics between the rising tube group, providing theoretical guidance and assistance for the design and operation of sCO<sub>2</sub> boilers.

### 1. Introduction

The application of sCO<sub>2</sub> cycle involves the fields of solar energy, coalfired power generation, etc., which have the characteristics of high efficiency, low-carbon, and high flexibility [1-3]. The research on improving the performance of sCO2 tubular heat exchangers has been carried out by many scholars (as shown in Table 1). Compared with the traditional water cycle, the CO2 cycle is easier to achieve and maintain ultra-supercritical (A-USC) status and is more inert, requiring lower material demands for pipe walls [8-10]. However, it has the disadvantages of higher required working fluid flow due to lower specific heat capacity and greater pressure drop [11,12]. Recent studies [13,14] have shown that modular sCO2 boilers can effectively solve the above problems. The cooling walls in the split-flow mode are more suitable for vertical tube screens, which can balance the outlet vapor temperature and reduce the pressure drop [15,16]. However, direct-flow boilers exhibit significant inter-tube thermal deviation along the furnace width direction [17], which promotes flow non-uniformity, resulting in large temperature differences between parallel tubes, inducing stress, and

potentially causing safety issues. Therefore, exploring the flow distribution characteristics and the matching law of heat source heat is one of the key research focuses of sCO<sub>2</sub> heat exchange cycle boilers.

In recent years, researchers at home and abroad have conducted numerous studies on the flow and heat transfer characteristics of working fluids such as water, R410A, and HFC32 mixed with HFC134a in parallel tube bundles. Bi et al. [18] studied SCC (high heat flux tubes can attract more flow) in the vertical upward parallel tubes of direct-through boilers at low mass flow rates during two-phase boiling of water. The results showed that at low inertial forces, the heated tubes often accompanied high flow rates. The strength of SCC was jointly affected by the pressure and the dryness of the working fluid in the tube. Miyata et al. [19] conducted experiments on the flow boiling of HFC32 and HFC134a in horizontally parallel channels with uneven heating, attempting to simulate the working conditions of air conditioning system heat exchangers. They eventually established an experimental correlation to predict the impact of uneven heating on flow distribution between channels, using variables such as the inlet dryness of the working fluid, the vapor-liquid density ratio, and the thermal deviation.

E-mail address: ehsun@ncepu.edu.cn (E. Sun).

<sup>\*</sup> Corresponding author.

**Table 1**Research Status of sCO<sub>2</sub> tubular heat exchanger.

References	Method	Geometry	Main finding
Khoshvaght- Aliabadi (2025) [4]	Numerical analysis	Vertical alternating Flattened Tubes	Using lower shaft angles can maximize the heat transfer efficiency of alternating flat tubes, with a 64.4% increase in heat transfer efficiency for downward flow and a 44.1% increase in heat transfer efficiency for upward flow.
Ghodrati (2024) [5]	Numerical analysis	Circular horizontal mini- tubes with tapered lateral profiles	Under the same conditions, the heat transfer coefficient in diverging microtubes is 5.2%~28.6% higher than that in converging microtubes, while the pressure drop decreases by 52.1% ~68.5%.
Liu (2025) [6]	Numerical analysis	Vertical circular tube with dimpled structures	The inline layout of elliptical concave pit tubes has better heat transfer performance than the staggered layout, the performance evaluation criterion (PEC) increases by 42.7% and 34.7% respectively.
Tang (2023) [7]	Experimental and numerical study	Vertical circular tube with conical strips insert	Pipes with conical strips inserts perform better than pipes with grooves or rectangular protrusions, and the performance evaluation criteria can reach 1.2 while preventing heat transfer deterioration.

Miglani et al. [20] studied the behavior of uneven flow distribution during the boiling process in horizontal double channels of water for the cooling performance of microchannels in electronic devices. The research showed that increasing thermal deviation between channels can only reduce the severity of uneven flow distribution to a certain threshold, beyond which there is no further reduction. At the same time, thermal coupling between tubes can mitigate the impact of uneven heating and promote uniform flow distribution. Zheng et al. [21] experimentally studied the flow distribution characteristics of sCO<sub>2</sub> in parallel heated tubes with an inner diameter of 2 mm. They concluded that in parallel tube bundles, high heat flux density tubes led to a decrease in mass flow rate due to density reduction and increased volumetric flow rate. They also assumed that the pressure drop in horizontal tube bundles is proportional to the square of the working fluid flow rate and established an sCO<sub>2</sub> flow distribution model.

Table 2 summarizes the flow distribution characteristics of various working fluids in the above literature. Due to the low density and low enthalpy of  $sCO_2$ , both SCC and reverse SCC are relatively weak. Existing research conclusions do not necessarily apply to  $sCO_2$ , such as why SCC only occurs under low mass flow conditions, why SCC first strengthens and then weakens with the increase of the working fluid dryness x in the tube, and why there is a threshold for the impact of thermal deviation on flow non-uniformity. The correlation between inter-tube heat distribution and flow distribution of  $sCO_2$  has not yet been established.

**Table 2**The influence of heat deviation on flow non-uniformity in reference literature.

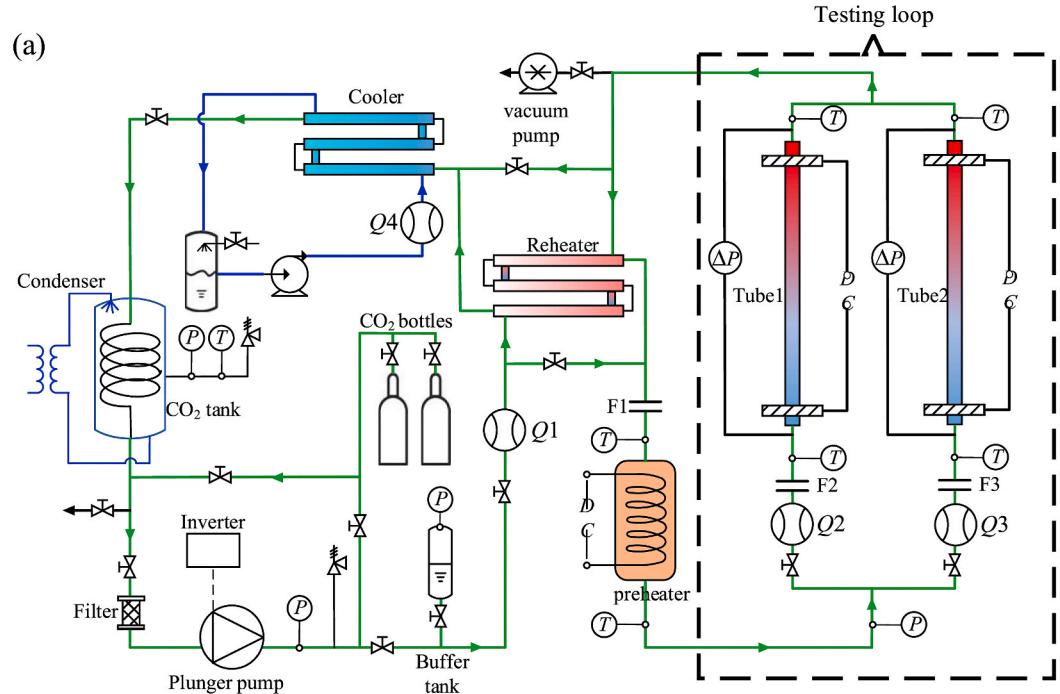
References	The parameter ranges	Specific impacts
Bi (2010) [14]	water, forced circulation, parallel vertical double pipes, $d_i = 15.4$ mm, $P = 11.3$ MPa $-21.5$ MPa, $G_{all} = 600$ kg/m <sup>2</sup> s $\sim 1000$ kg/m <sup>2</sup> s, $q_w = 50$ kW/m <sup>2</sup> $\sim 140$ kW/m <sup>2</sup> , $\varphi = 1.25 - 3.00$ .	Flow distribution characteristics show SCC, with inter-tube heat deviation increasing by 200%, resulting in a maximum mass flow rate increase of 42.33%.
Miyata (2020) [15]	HFC32 and HFC134a, forced circulation, parallel horizontal double pipes, $l_i=0.5$ mm, $P=0.414$ MPa $\cdot$ 1.017 MPa, $G_{\rm all}=100$ kg/m <sup>2</sup> s $\sim$ 200 kg/m <sup>2</sup> s, $q_{\rm w}=1.5$ kW/m <sup>2</sup> $\sim$ 7 kW/m <sup>2</sup> , $\varphi=0.29-1.00$ .	Flow distribution characteristics show inverse SCC, with intertube heat deviation increasing by 71%, resulting in a maximum mass flow rate decrease of 17.25%.
Miglani (2021) [16]	water, natural circulation, parallel horizontal double pipes, di = 1 mm, $P = 1.044$ MPa, $G_{\rm all} = 0{\sim}1000 \text{ kg/m}^2\text{s}$ , $q_{\rm w} = 12.73 \text{ kW/m}^2{\sim}50.93 \text{ kW/m}^2$ , $\varphi = 0$ , $2/1$ , $1/0$ .	Flow distribution characteristics show inverse SCC, with single tube heating leading to a maximum mass flow rate decrease of 97.4%.
Zheng (2022) [17]	CO <sub>2</sub> , forced circulation, parallel horizontal double pipes, $d_i = 2$ mm, $P = 7.5$ MPa $\sim$ 9.5 MPa, $G_{\rm all} = 530.52$ kg/m <sup>2</sup> s $\sim$ 1061.04 kg/m <sup>2</sup> s, $q_{\rm w} = 55$ kW/m <sup>2</sup> $\sim$ 400 kW/m <sup>2</sup> , $\varphi = 0\sim$ 6.	Both SCC and reverse SCC phenomena occur. The thermal deviation can cause fluctuations in the flow rate of the tube from $-12.56\%$ to $1.78\%$

The purpose of this paper is to relate heat displacement to uneven flow distribution from the perspective of fluid force analysis. By introducing the pseudo-boiling theory [22-24], the K number is used to characterize the effect of vapor-like (VL) layer thickness accumulation and reduced flow cross-sectional area obstructing the main flow (orifice throttling effect, referred to as OCE) during the pseudo-boiling heat exchange process, Re is used to reflect the influence of viscosity between fluid molecules on flow, and the Bu number is used to characterize the promoting effect of buoyant force caused by the temperature field on the main flow. Ultimately, a predictive correlation between heat distribution and flow distribution in the parallel tube bundle of vertical upward flow of sCO<sub>2</sub> is established. In addition, the research background of this article is focused on the dynamic adjustment process of boiler start-up and shutdown or the CO2 transcritical Rankine cycle. The start-up and shutdown process is generally very slow (taking several hours to complete), and can be approximated as a steady state. At this time, the range of operating parameters is very large (room temperature~500 °C and CO<sub>2</sub> local critical pressure~30 MPa) [25,26]. The operating parameters of CO<sub>2</sub> transcritical Rankine cycle generally fluctuate within the range of room temperature~300 °C and 4 MPa~20 MPa [27,28]. Under the background of the above-mentioned engineering applications, the study of thermal deviation on flow distribution characteristics is carried out in combination with existing experimental conditions.

#### 2. Experimental apparatus and data reduction

# 2.1. Experimental system

The experimental system is shown in Fig. 1, including the cooling circulation loop, forced convection loop, DC heating system, and operating parameter measurement loop. Before the experiment, the  $\rm CO_2$  convection loop is vacuumed to remove non-condensable gases and filled with  $\rm CO_2$  of 99.99% purity. The  $\rm CO_2$  liquid is driven by a plunger pump, then heated to the required temperature in the recuperator heat exchanger and preheater before entering the testing loop. The preheater and experimental tubes 1 and 2 are heated by independent DC transformers with maximum rated powers of 54 kW, 120 kW, and 60 kW, respectively. As shown in Fig. 2(a), due to the limitation of site space and



Plunger pump tankF:Insulation flange P: Pressure sensor T: Thermocouple  $\Delta P$ : Differential pressure sensor DC:

Direct current transformer Q: Mass flow meter

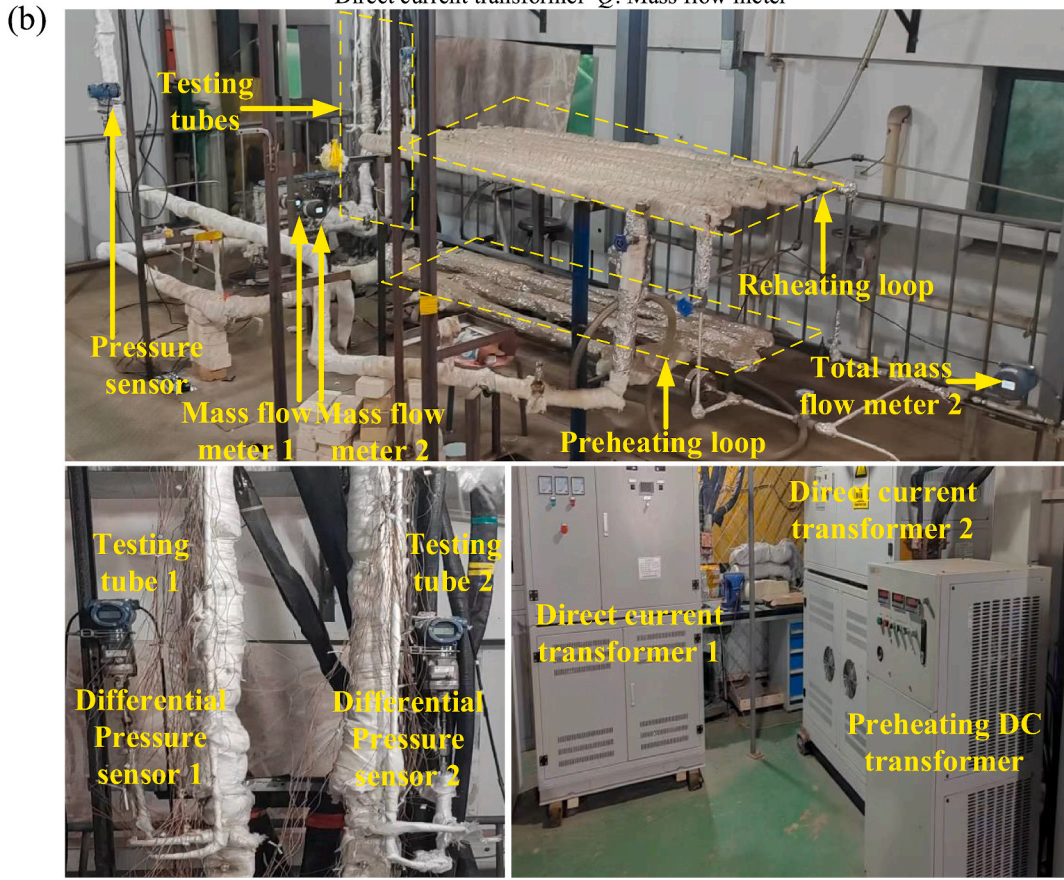


Fig. 1. Experimental System Diagram (a: Schematic diagram of the experimental loop, Green Line—CO<sub>2</sub>, Deep Blue Line—Water, Light Blue Line—Ethylene Glycol; b: photo of experimental system). (For interpretation of the references to colour in this figure legend, the reader is referred to the Web version of this article.)

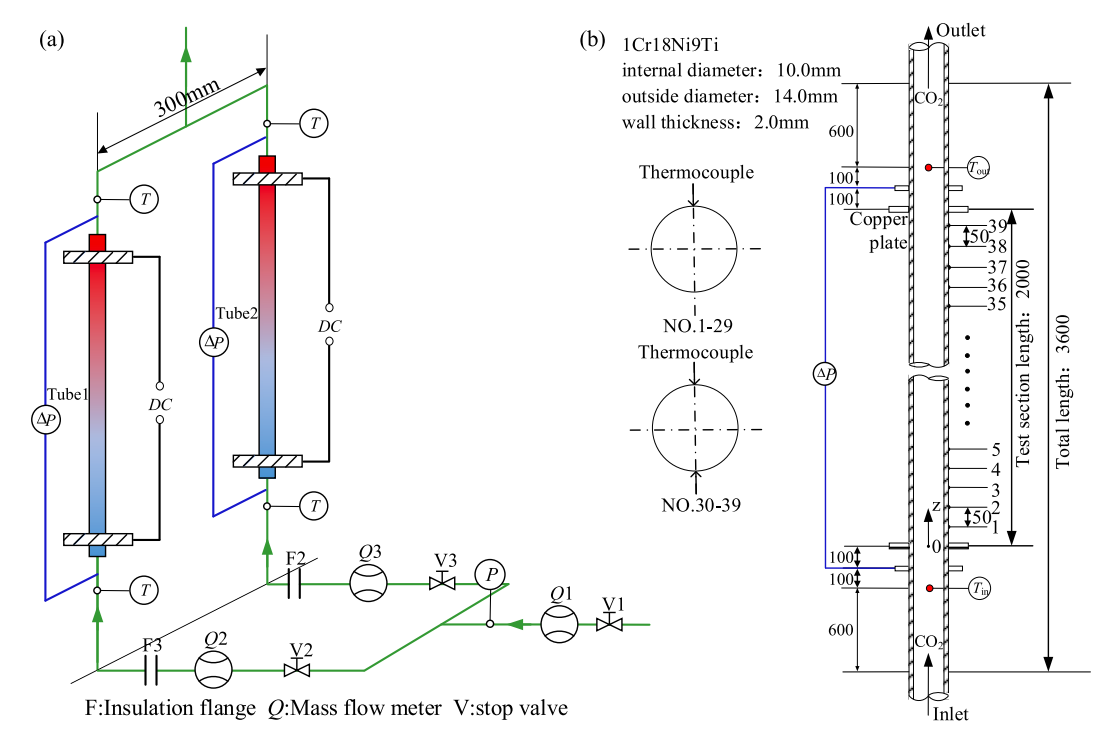


Fig. 2. Testing loop (a: Symmetrical "L"-shaped pipeline layout, b: Testing loop pipeline structure).

without affecting the experimental results, the parallel double-pipes in the experimental section are arranged in a symmetrical "L"-shape. Each branch pipeline is equipped with a throttle valve, a mass flow meter, and an insulation flange at the same position as the horizontal pipeline, and is equipped with a DC heating power supply to achieve independent control of the heating power of each pipeline, providing a prerequisite for the controllable thermal deviation between pipelines. At the outlet of the testing loop,  $\rm CO_2$  vapor is continuously cooled by the recuperative heat exchanger, cooler, and condenser. The coolant in the cooling loop cooler is ambient water, and the condenser uses a glycol-water solution with a freezing point of  $-35~\rm ^{\circ}C$  to cool the  $\rm CO_2$  to 1  $\rm ^{\circ}C$ , ensuring high density of the working fluid in the high-pressure storage tank before the pump, thus ensuring the pump's delivery capacity during continuous experiments.

#### 2.2. Test tube

Fig. 2(b) shows a pipeline made of 1Cr18Ni9Ti material, with an outer diameter of 14 mm and an inner diameter of 10 mm. The layouts of tubes 1 and 2 are identical, with a total length of 3600 mm, including two 800 mm stable sections at the ends and a 2000 mm main testing loop in the middle. These thermocouples are arranged in 39 cross-sections along the flow direction. The axial distance between adjacent crosssections is 50 mm. There is one thermocouple in Cross-sections 1-29. Since the thermocouple wires in the high-temperature area of the pipe wall are prone to falling off, resulting in data distortion. To improve the reliability of the measured data, two thermocouples are arranged in Sections 30-39. The pipeline is wrapped with insulation material of extremely low thermal conductivity, resulting in almost identical readings from two thermocouples at the same cross-section under geometric symmetry. The temperature measured in the experiment mainly refers to the outer wall temperature and inlet/outlet temperature of the experimental section. The outer wall temperature is measured using an OMEGA 0.25 mm K (NiCr-NiSi) thermocouple wire, which is fixed to the outer wall of the tube using a capacitive impact welding machine. Therefore, there is no contact thermal resistance between the thermocouple wire and the outer wall of the tube. The inlet and outlet temperatures of the experimental section were measured using a 3 mm OMEGAK type (NiCr-NiSi) armored thermocouple. The armored thermocouple was vertically inserted into the center of the tube and connected to a self-designed thermocouple socket to achieve high voltage sealing.

Before each inter tube thermal deviation experiment, it is necessary to adjust the opening of the throttle valve on the test circuit to ensure a uniform distribution of flow between tube 1 and tube 2 without tubes thermal deviation, minimizing the impact of pipeline structure on flow distribution. System reliability is verified (see Fig. 3), with experimental results being repeatable under the same operating parameters, and the wall temperature and mass flow rates of tubes 1 and 2 are symmetrically distributed without setting inter-pipe thermal deviation.

The local wall temperatures along the tube are measured by fiftynine 0.5 mm K-type thermocouple wires with an accuracy of  $\pm 0.5$  °C. The inlet and outlet temperatures of sCO<sub>2</sub> are measured with two K-type sheathed thermocouples with an accuracy of  $\pm 0.5$  °C. The inlet pressure is measured by an Rosemount 1151 pressure transducer with an accuracy of  $\pm 0.2\%$  and the pressure drop over the test tube is measured by a Rosemount 3051CD2 differential pressure transducer with an accuracy of  $\pm 0.1\%$ . The mass flux into the tube is measured via a DMF-1-3 Coriolis-mass-flow meter with an accuracy of  $\pm 0.2\%$  and test range of 0~600 kg/h (corresponding to mass flux G = 0~2122 kg/m<sup>2</sup>s). All signals are collected by ADAM-4117/4118 and ultimately collected by Advantech 610L industrial control computer for real-time supervision and recording. The uncertainties of heat flux and the uneven errors in initial flow rate and resistance between tubes 1 and 2 caused by the processing and installation of the pipeline itself are calculated [29]:

$$\delta R = \sqrt{\left(\frac{\partial R}{\partial x_1}\delta x_1\right)^2 + \left(\frac{\partial R}{\partial x_2}\delta x_2\right)^2 + \dots + \left(\frac{\partial R}{\partial x_n}\delta x_n\right)^2}$$
 (1)

where R is the derived quantity, and  $\delta x_1$ ,  $\delta x_2$  ...  $\delta x_n$ , represent the uncertainties of independent parameters of  $x_1$ ,  $x_2$  ...  $x_n$ , respectively. Both the test ranges and uncertainties of the experimental parameters are listed in Table 3.

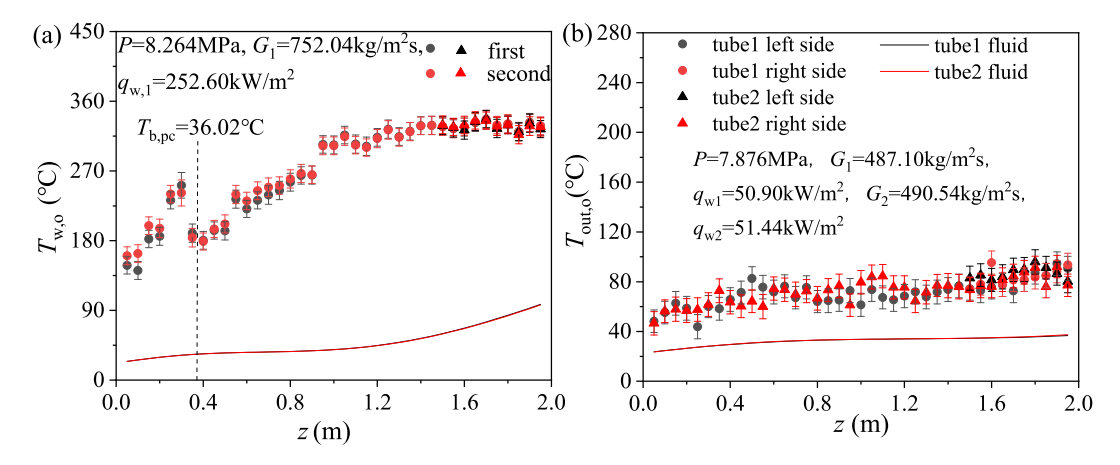


Fig. 3. Reliability testing experiment (a: Repeatability testing experiment, b: parameter symmetry detection experiment).

**Table 3**Parameter measurements and uncertainties.

Parameters	Range	Uncertainty
Pressure P (MPa)	7.5~15	1.0%
Total differential pressure $\Delta P_{\text{all}}$ (kPa)	8.6~19.6	2.06%
Inlet fluid temperature $T_{in}$ (°C)	22~28	0.5 °C
Outlet fluid temperature $T_{\text{out}}$ ( $^{\circ}$ C)	33~294	0.5 °C
Outer wall temperature $T_{w,out}$ (°C)	34~568	0.5 °C
Total mass flux $G_{all}$ (kg/m <sup>2</sup> s)	600~1400	2.05%
Heating power of single tube $P_c$ (kW)	$3.1 \sim 22.0$	0.28%
Heat flux of single tube $q_w$ (kW/m <sup>2</sup> )	50~350	2.61%
Flow distribution ratio of tube 1 when $\varphi = 1$ $\delta_{1, \varphi = 1}$	0.996~0.999	2.90%
The ratio of inter tube resistance without thermal deviation $R_1/R_2$	1.01~1.04	4.60%

#### 2.3. Date reduction

According to the experimental system, the experimental pipe with the inner wall heat flux equal to the average heat flux under the given conditions is called the compensation pipe, while the other experimental pipe is called the deviation pipe. The thermal deviation is defined as the ratio of the inner wall heat flux of the deviation pipe to that of the compensation pipe, and the specific expression of  $\varphi$  is as follows [18]:

$$\varphi = \begin{cases} \frac{q_{\text{w.2}}}{q_{\text{w.1}}}, \varphi \le 1\\ \frac{q_{\text{w.1}}}{q_{\text{w.2}}}, \varphi > 1 \end{cases}$$
 (2)

Where  $\varphi$  is the thermal deviation,  $q_{\rm w,1}$  is the inner wall heat flux of tube 1, and  $q_{\rm w,2}$  is the inner wall heat flux of tube 2.

The flow distribution characteristics of parallel pipelines are described using the flow distribution ratio which is defined as follows [21]:

$$\delta_1 = \frac{G_1}{G_{\text{ave}}} = \frac{G_1}{G_{\text{all}}/2} \tag{3}$$

$$\delta_2 = \frac{G_2}{G_{\text{ave}}} = \frac{G_2}{G_{\text{all}}/2} \tag{4}$$

Where  $\delta_1$ ,  $\delta_2$  are the distribution ratio of the working fluid flow through pipes 1 and 2, respectively;  $G_1$  and  $G_2$  are the mass flow velocities of the working fluid passing through pipes 1 and 2, respectively;  $G_{\rm ave}$  is the average mass flow rate of the working fluid through the testing loop's branch pipelines, and  $G_{\rm all}$  is the mass flow rate of the working fluid through the main pipeline.

For vertically upward flowing electric heating circular tubes, it is assumed that the heat flux density is uniformly distributed. In addition,

due to the small heat loss from the experimental section pipeline to the outside during the electric heating experiment, the heat loss under most operating conditions is within 1% (see Fig. 4), which is determined by the following equation  $q_w$  [21]:

$$q_{\rm w} = \frac{\eta_{\rm th} P_{\rm c}}{\pi d_{\rm in} L} \tag{5}$$

Where  $q_w$  is the Single tube heat flux,  $P_c$  is the heating power,  $d_i$  is the inner diameter of the testing loop tube wall,  $\eta_{th}$  is the average thermal efficiency, with a value of 0.996.

To match the arrangement of the thermocouple wire measurement points, the total length L of the experimental section is divided into 40 sections along the axial z. Then, using the NIST standard database [22], the state or physical properties of the fluid at corresponding positions are estimated based on the average enthalpy  $i_b(z)$  of the working fluid in each section, such as mainstream temperature  $T_b(z)$ , density  $\rho_b(z)$ , thermal conductivity  $\lambda(z)$ , dynamic viscosity  $\eta(z)$ , etc. Given the inlet mainstream temperature  $T_{b,in}$  and mass flow rate G, it is assumed that the enthalpy rise of the working fluid increases linearly along the axial direction of the heating section. By energy conservation, we have [29]:

$$P_{c} = \int \rho_{b} u i(z + dz) 2\pi r dr - \int \rho_{b} u i(z) 2\pi r dr$$
 (6)

Simplification can lead to Ref. [29]:

$$\pi \mathbf{d}_{i} q_{w} \mathbf{d} x = \dot{m} [i(z + \mathbf{d} z) - i(z)]$$
(7)

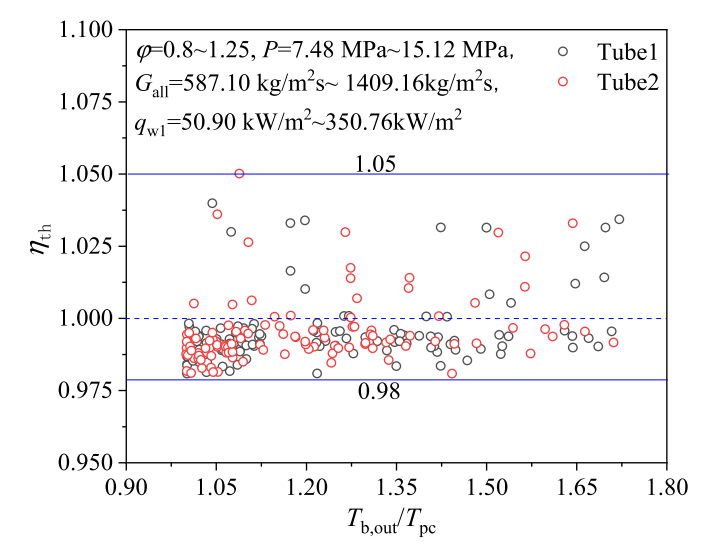


Fig. 4. Thermal equilibrium.

The expression for quality flow rate here is [29]:

$$\dot{m} = \int \rho_b u 2\pi r dr = G \frac{\pi}{4} d_i^2 \tag{8}$$

Where  $\dot{m}$  is the single tube mass flow rate, z is the coordinates along the axis of the pipeline, i is the Enthalpy value of working fluid  $\mathrm{CO}_2$  at corresponding temperature,  $\rho_{\mathrm{b}}$  is the mainstream local density, u is the flow velocity of the fluid element along the length direction of the pipe, r is the radial distance between the fluid element and the center of the circle in the current section, and G is the mass flow velocity of the fluid working fluid.

The enthalpy value at any point z along the length direction of the tube is [30]:

$$i_{b}(z) = i_{b,in} + \frac{4q_{w}z}{Gd_{i}} \tag{9}$$

The expression for the layout temperature  $T_{w,i}(z)$  of the inner wall of the pipeline during the steady-state process is [30]:

$$T_{\rm w,i}(z) = T_{\rm w,o}(z) - \frac{q_{\rm w,i}d_{\rm i}}{4\lambda(z)} \bigg(\frac{a^2-2\, ln\, a-1}{1-a^2}\bigg), \bigg(a = \frac{d_{\rm i}}{d_{\rm o}}\bigg) \eqno(10)$$

Where  $T_{\rm w,i}$  is the temperature of the inner wall of the testing loop,  $T_{\rm w,o}$  is the temperature of the outer wall of the testing loop, and  $d_{\rm o}$  is the outer diameter of the testing loop wall.

#### 3. Results and discussion

# 3.1. Effects of various parameters on flow distribution

In this paper, the parameter ranges of P, G,  $q_{\rm w}$  and  $\varphi$  are 7.5 MPa~15 MPa, 600 kg/m²s~1400 kg/m²s, 50 kW/m²~350 kW/m², and 0.8~1.25, respectively (the value range of  $\varphi$  is referenced from Refs. [11,31]). The effects of various parameters on the flow distribution in parallel tubes are investigated, where the thermal deviation has negligible influence on the total flow through the parallel tubes. The heat and flow ratio between testing loop tube 1 and tube 2 are interlinked (reference equations (2)–(4)), and the parameters of a single tube are sufficient to express the changes under different working conditions. Therefore, the result analysis below is presented using the data from tube 1 (e.g.  $q_{\rm w,1}$ ,  $\delta_1$ ,  $SBO_1$ ,  $x_{\rm out,1}$ ).

Fig. 5 shows the effects of heat flux density on the flow distribution of tube 1 and tube 2 under different pressures and thermal deviations. When the heat flux is small, the high heat flux tube can attract more flow (SCC plays a dominant role), and when the heat flux is large, the low heat flux tube carries more flow (OCE plays a dominant role). Fig. 5(a)

indicates that in high heat flux conditions, increasing the pressure helps achieve a more uniform flow distribution between the tubes. The increased enthalpy slows down the buildup of pseudo-film thickness, delaying the occurrence of OCE [30]. Staying away from the critical pressure under high heat flux conditions helps maintain the uniform of wall temperatures between the tubes, ensuring the safe operation of the boiler. The increase in the critical SBO<sub>1</sub> number [29] for the transition from SCC to OCE with increasing pressure is a good proof of this. Fig. 5 (b) shows that the deviation value of heat and the extent of flow transfer are not completely positively correlated. When the thermodynamic dryness [22,32] at the outlet of tube 1 is  $x_{out,1} < 0.54$  or  $x_{out,1} > 1.44$ , the larger the heat deviation between the tubes, the more uneven the flow distribution. However, when it is  $0.54 < x_{out,1} < 1.44$ , the larger the heat deviation between the tubes, the more it alleviates the unevenness of the flow distribution. This is due to the sudden increase in the volume expansion coefficient  $\alpha_v$  of sCO<sub>2</sub> during the pseudo-boiling

Generally, when other parameters remain unchanged, an increase in the total flow rate leads to a reduction in the heat shared per unit mass of fluid. This weakens the effect of heat non-uniformity, making the flow distribution more uniform. This trend is evident in Fig. 6, where  $\delta_1$  approaches 1 as  $G_{\text{all}}$  increases. However, this conclusion is valid only if the thermal properties of the fluid do not change drastically. When the ratio of pressure to critical pressure  $P/P_{cr} < 2.71$ ,  $\alpha_{v}$  increases sharply during the pseudo-boiling process until it reaches a superheated state (x > 1), after which  $\alpha_v$  decreases and stabilizes. As  $x_{out}$  approaches 1, the buoyancy force on the fluid in the heating tube increases due to the fluctuation of  $\alpha_v$ . This enhances the attraction of high heat flow pipes to the fluid flow, explaining the flow rate rebound in pipe 1 around 1000  $kg/m^2s$  of  $G_{all}$  in Fig. 6(a). Additionally, the heat deviation between pipes in Fig. 6(b) is smaller, indicating less influence from changes in fluid properties. Overall, as the fluid dryness decreases, the flow distribution between pipes becomes more uniform.

Figs. 7 and 8 illustrate the matching rules of heat and flow under different heat flux densities and mass flow rates. The flow rate may not be completely even, and as the heat flux density increases,  $\delta_1$  slightly decreases and remains around 0.997. This is influenced by the pipe structure and does not affect the analysis and exploration of these rules. Comparing the fluctuation range of  $\delta_1$  in Fig. 7(a) and (b), it is found that increasing the pressure from 7.5 MPa to 12 MPa results in the fluctuation range of the flow rate in a single pipe changing from -5.64%-1.00% to -4.08%-1.25%. This indicates that increasing the pressure improves the OCE phenomenon. Moreover, increasing pressure promotes SCC by enhancing the density difference between VL and liquid-like (LL) phases, resulting in greater buoyancy in high heat flow pipes. This is well reflected in the pressure drop changes in Fig. 9. Additionally, under far

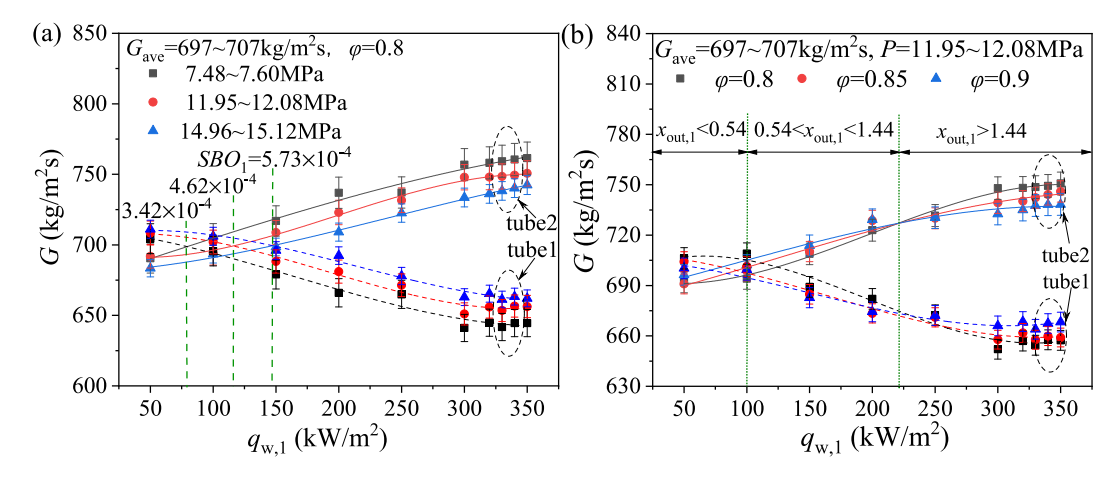


Fig. 5. The influence of operating parameters on the mass flow velocity of testing loop tube 1 and tube 2 (a: the influence of pressure, b: the influence of thermal deviation).

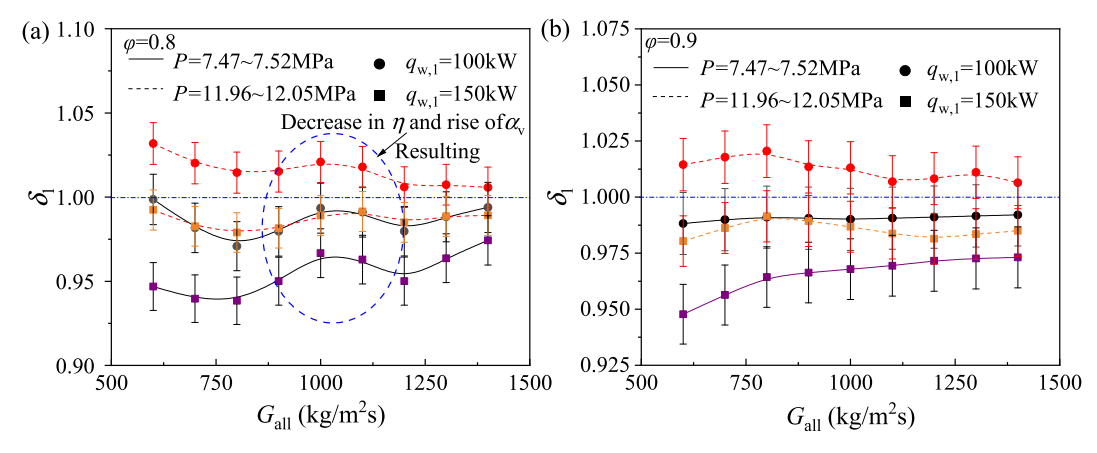


Fig. 6. The influence of mass flow rate on the flow distribution characteristics of parallel pipes (a: under high heat deviation, b: under low heat deviation).

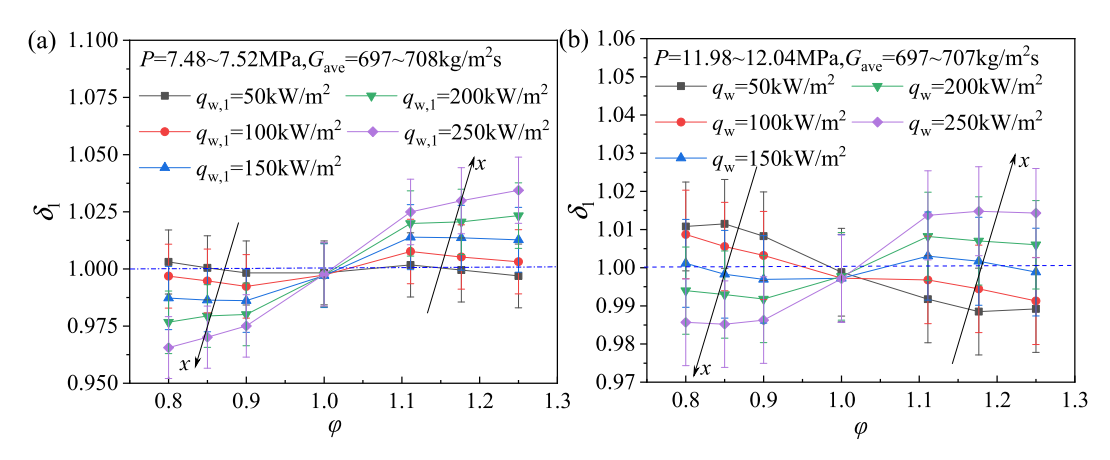


Fig. 7. Matching law of heat and flow rate under different heat flux densities (a: under near critical pressure, b: at far critical pressure).

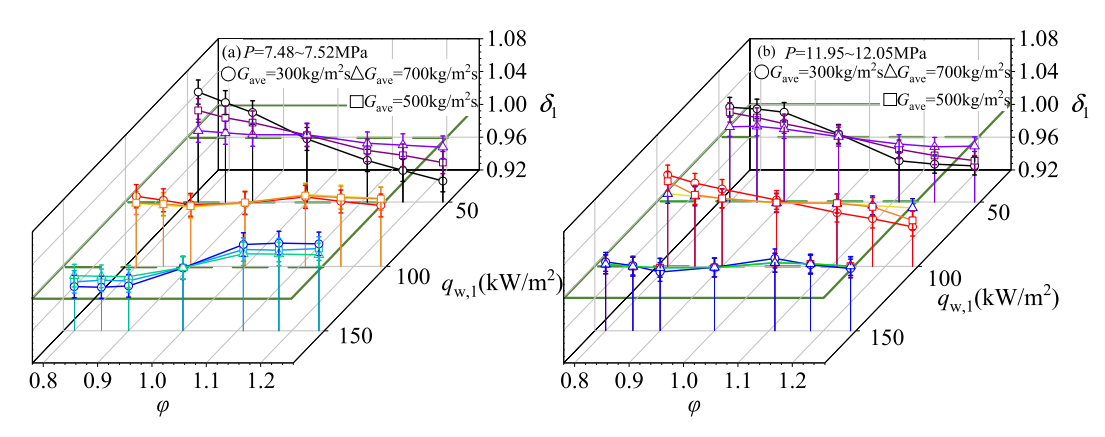


Fig. 8. Matching law of heat and flow rate under different mass flow rates (a: under near critical pressure, b: at far critical pressure).

critical pressure conditions, a 15% heat shift causes more severe flow non-uniformity than a 20% heat shift, which is due to the enhancement of SCC as the heat shift increases when  $x_{out,1}$  is small, similar to the law of water [33]. In addition, due to the errors in initial flow rate and resistance caused by the processing and installation of the pipeline itself, there is also a slight deviation in the flow rate between the pipes when there is no thermal deviation. Therefore, when  $\varphi=1$ , the vertical axis of the inflection point of the curve in Fig. 7 is close to 1 but not equal to one, which is a normal phenomenon.

Fig. 8 provides a clearer illustration of the transition process from SCC to OCE in sCO<sub>2</sub> compared to Fig. 7. Near the critical point, when  $q_{\rm w,1}/G_1 > 0.14$  the back fluid no longer exhibits natural circulation flow

characteristics due to the influence of steam driving force, where stronger heating of the pipeline results in less flow distribution. At a far critical point, when  $q_{\rm w,1}/G_1>0.21$  the buoyancy force on the back fluid no longer dominates, and the OCE phenomenon is delayed by the influence of pressure. This corroborates the conclusion in Fig. 5(a) that the critical  $SBO_1$  number of flow distribution is positively correlated with pressure. It is noteworthy that even under conditions where uneven heating causes negative feedback in flow rate, the effect of buoyancy force does not disappear, which explains why in Fig. 8, all conditions exhibiting OCE did not achieve the maximum flow deviation at the extreme value of thermal deviation  $\varphi$ .

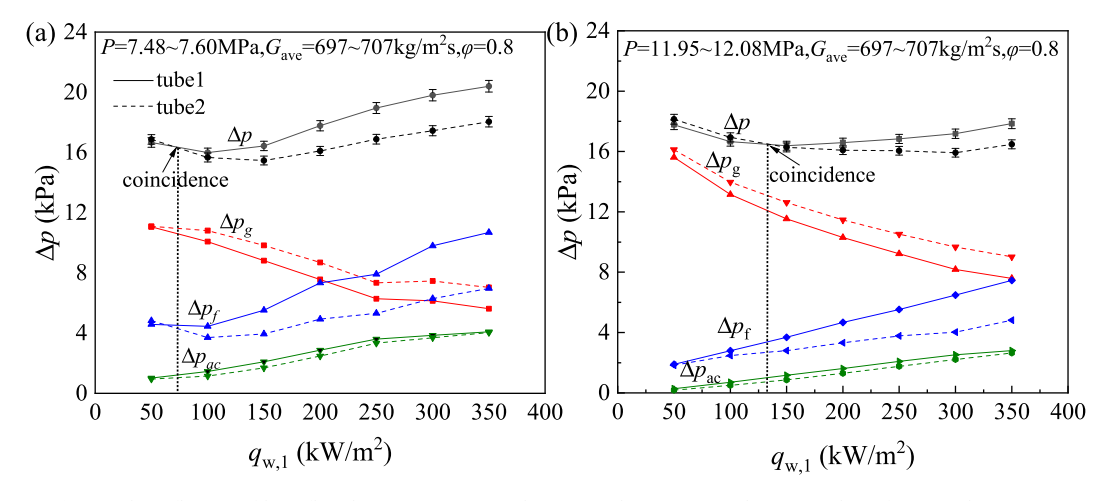


Fig. 9. The influence of heat flux density on pressure drop (a: under near critical pressure, b: at far critical pressure).

#### 3.2. Parallel vertical flow distribution model

The pressure drop changes in experimental tubes 1 and 2 during the heating process were monitored, and the results are shown in Fig. 9. The total pressure drop in the heating sections of tubes 1 and 2 is not equal due to local pressure losses caused by mass flow meters and throttle valves (estimated by the principle of equal pressure drop in parallel pipes, its relative position is shown in Fig. 1), which is normal and reasonable. Additionally, as the heat flux density increases, it first decreases and then increases, with frictional pressure drop and acceleration pressure drop gradually increasing and gravitational pressure drop gradually decreasing. The increase in frictional pressure drop and the decrease in gravitational pressure drop together determine the change trend of the total pressure drop in the heating section. It is noteworthy that the coincident point of the total pressure of tubes 1 and 2 is consistent with the coincident point of flow rate in Fig. 5(a), indicating a negative correlation between flow distribution and pressure drop distribution. The smaller the flow resistance in the heating pipe, the greater the flow distribution, which can be predicted by the pressure drop ratio relationship to determine the state (SCC or OCE) of the flow distribution [20,34,35]. Therefore, theoretical calculations of flow pressure drop inside the pipes were conducted to attempt to predict the flow ratio between tubes.

Due to the parallel connection of tubes 1 and 2 in the testing loop, there exists the following relationship [21]:

$$\Delta P_1 = \Delta P_2 = \Delta P_t + \Delta P_L \tag{11}$$

$$\Delta P_{\rm t} = \Delta P_{\rm ac} + \Delta P_{\rm g} + \Delta P_{\rm f} \tag{12}$$

Where  $\Delta P_1$ ,  $\Delta P_2$  are the total pressure drop of testing loop tube 1 and 2, respectively; and  $\Delta P_t$  is the pressure drop measured by the differential pressure transmitter in the heating testing loop,  $\Delta P_{ac}$  is the accelerated pressure drop of fluid flow,  $\Delta P_g$  is the gravitational pressure drop caused by gravity,  $\Delta P_f$  is the frictional pressure drop caused by the viscosity.

 $\Delta P_{\rm ac}$  defined by the following equation [30]:

$$\Delta P_{\rm ac} = \rho_{\rm b,out} u_{\rm out}^2 - \rho_{\rm b,in} u_{\rm in}^2 = G^2 \left( \frac{1}{\rho_{\rm b,out}} - \frac{1}{\rho_{\rm b,in}} \right)$$
 (13)

Where  $\rho_{\rm b,out}$  is the density of the working fluid at the outlet of the testing loop, is the density of the working fluid at the outlet of the testing loop,  $\rho_{\rm b,in}$  is the flow velocity of the fluid element along the length direction of the pipe, and G is the average mass flow velocity of the working fluid in tube 1 or tube 2.

 $\Delta P_{\rm g}$  is defined by the following equation [30]:

$$\Delta P_{\rm g} = \int_0^{\Delta H} \rho_{\rm b} g \sin \theta dx = g \rho_{\rm b,ave} \Delta H \sin \theta \tag{14}$$

Where  $\rho_{\rm b,ave}$  is the average value of the local working fluid density for 40 sections, g is the gravitational acceleration, with a value of 9.8 m/s<sup>2</sup>,  $\Delta H$  is the height difference between the upper and lower parts of the testing loop pipeline,  $\theta$  is the angle between the testing loop pipeline and the horizontal line, the value for the vertical pipe group is  $\pi/2$ .

 $\Delta P_f$  can be defined by the following equation [30]:

$$\Delta P_{\rm f} = f \frac{\rm L}{\rm d_i} \frac{G^2}{2\rho_{\rm b,ave}} \tag{15}$$

Where the friction coefficient *f* is recorded in Table 4.

The local pressure drop mainly caused by local blockage of the mass flow meter and throttle valve  $\Delta P_L$  can be defined by the following equation [30]:

$$\Delta P_{\rm L} = \varepsilon \frac{G^2}{2\rho_{\rm hin}} \tag{16}$$

Assuming that the  $\varepsilon$  of tubes 1 and 2 are the same, the simultaneous formulas (10) and (18) can be derived as follows [21]:

$$\Delta P_{\rm L,2} - \Delta P_{\rm L,1} = \Delta P_{\rm t,1} - \Delta P_{\rm t,2} = \varepsilon \frac{{G_2}^2 - {G_1}^2}{2\rho_{\rm b,in}}$$
 (17)

Where  $\rho_{\rm b,in}$  is the density of working fluid at the entrance of the experimental section,  $\varepsilon$  is the local resistance coefficient, according to the linear fitting of experimental data in Fig. 10, the value is 23.44.

For these two channels, substitute formulas (2) - (3), (11) - (14), and (18) into equation (10) to obtain the relationship equation of mass flow rate ratio between the two parallel tubes:

$$\delta_1^2 \left( \frac{f_1 L}{2 d_i} + \frac{\varepsilon}{2 \rho_{\text{bin } 1}} \right) - \delta_2^2 \left( \frac{f_2 L}{2 d_i} + \frac{\varepsilon}{2 \rho_{\text{bin } 2}} \right) = \frac{g L \left( \rho_{\text{b,ave}, 2} - \rho_{\text{b,ave}, 1} \right)}{G_{\text{ave}}^2}$$
(18)

And because of the existence of a relationship:  $\delta_1+\delta_2=2$ , simultaneously assuming  $c_1=\frac{f_1L}{2d_i}+\frac{\varepsilon}{2\rho_{\mathrm{b.in.}1}}$ ,  $c_2=\frac{f_2L}{2d_i}+\frac{\varepsilon}{2\rho_{\mathrm{b.in.}2}}$ ,  $b=\frac{\mathrm{gL}(\rho_{\mathrm{b.ave.}2}-\rho_{\mathrm{b.ave.}1})}{G_{\mathrm{ave}}^2}$ . Finally, the flow distribution ratio of tube 1 can be derived from formula (18) as follows:

$$\delta_{1} = \begin{cases} -\frac{2c_{2}}{c_{1} - c_{2}} + \sqrt{\frac{b + 4c_{2}}{c_{1} - c_{2}} + \frac{4c_{2}^{2}}{(c_{1} - c_{2})^{2}}}, c_{1} - c_{2} > 0 \\ -\frac{2c_{2}}{c_{1} - c_{2}} - \sqrt{\frac{b + 4c_{2}}{c_{1} - c_{2}} + \frac{4c_{2}^{2}}{(c_{1} - c_{2})^{2}}}, c_{1} - c_{2} < 0 \end{cases}$$

$$(19)$$

**Table 4**Available friction factor correlations in references.

References	correlations	The parameter ranges
Filonenko (1954) [36]	$f = (1.82 log_{10} Re - 1.64)^{-2}$	Single-phase flow, $10^4 \le Re \le 5 \times 10^6$
Petukhov (1983) [37]	$f = (1.82 log_{10} Re - 1.64)^{-2} \left(\frac{\mu_{\rm w}}{\mu_{\rm h}}\right)^{0.24}$	Based on data of sCO $_2$ with P = 7.7 MPa/8.9 MPa $q_{\rm w}=384$ kW/m $^2\sim1053$ kW/m $^2$ , $G=1000$ kg/m $^2$ s $\sim4100$ kg/m $^2$ s, $d_{\rm i}=8$ mm
Fang (2020) [38]	$f = 0.0127 \left[ ln \left( 650 \left( \frac{\varepsilon_{\text{ave}}}{d_{\text{i}}} \right)^{0.67} + \left( \frac{99000}{\text{Re}} \right)^{1.32} + 0.066\text{Ch} \right) \right],$	Based on data of $\mathrm{CO}_2$ , R22, R404A, R134a, R410A, RP-3 and $\mathrm{H}_2\mathrm{O}$
	$Ch = rac{P}{G\sqrt{i-i_0}}$	
Zhang (2021) [30]	$f = 2.15Re^{-0.342}K^{0.027}, K = \left(\frac{q_{\rm w}}{Gi_{\rm w}}\right)\frac{\rho_{\rm VL}}{\rho_{\rm LL}}$	Based on sCO <sub>2</sub> data with $P=7.5$ MPa–23 MPa, $Re=3.38\times10^4$ –6.29 $\times$ $10^5$ , $T_{\rm b}=10$ °C–200 °C, $d_{\rm i}=8$ mm/10 mm/12 mm
Lv(2022) [39]	$rac{f}{f_{ m Filo}}=1.34igg(rac{\mu_{ m w}}{\mu_{ m b}}igg)^{0.315}igg(rac{ ho_{ m w}}{ ho_{ m b}}igg)^{-0.104},$	Based on sCO $_2$ data with $P=7.62$ MPā8.44 MPa, $G=600$ kg/m $^2$ s $\sim \!1600$ kg/m $^2$ s, $q_{\rm w}=49.3$ kW/m $^2\sim \!152.3$ kW/m $^2$ ; $d_{\rm i}=2$ mm
Hao (2023) [40]	$f_{\text{Filo}} = (0.79 \ln Re - 1.64)^{-2}$ $f = 1.1228 Re_{ave}^{-0.287} x_{ave}^{-0.027}$	Based on CO <sub>2</sub> data with $P=5.51$ MPa–20.41 MPa, $Re=3.44\times 10^4$ –4.25 $\times$ $10^5$ , $T_b=8.29$ °C–231.56 °C, $d_i=8$ mm

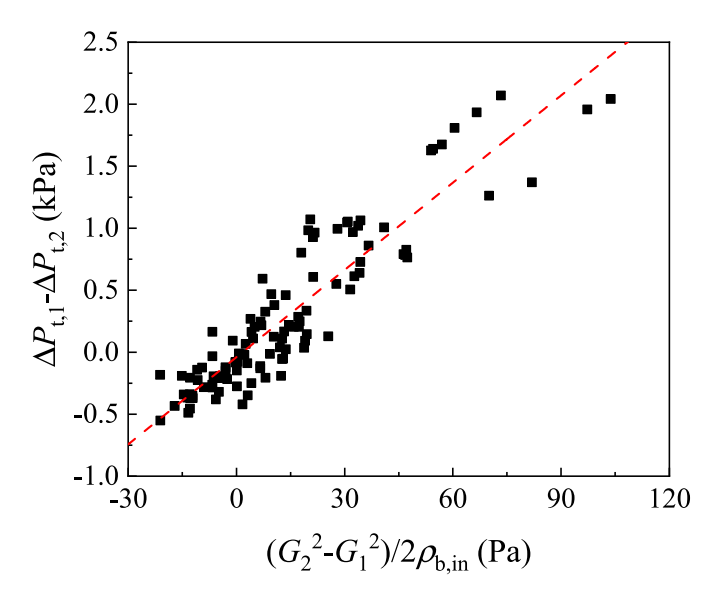


Fig. 10. Fitting of local resistance coefficient  $\epsilon$ .

A predictive model for flow distribution in parallel vertical dual pipelines was established, and the correlation of the predictive results was calculated using formulas (22) and (23). As shown in Fig. 11, among the six different friction coefficient correlation prediction equations [30, 36–40], only equations (b) and (e) that consider the influence of viscous forces inside the pipe have good prediction accuracy for flow distribution ratio. However, there is also a root mean square error of at least 1.41%, indicating poor correlation. It is necessary to analyze and quantify the underlying mechanism to further enhance the accuracy of prediction.

For the flow distribution ratio  $\delta_1$ , the error of a single data point is [40]:

$$e = \frac{\delta_{\text{pre}} - \delta_{\text{exp}}}{\delta_{\text{exp}}} \tag{20}$$

Meanwhile, the relationship between the size of the following three discrimination errors is defined [40]:

$$e_{\rm A} = \frac{1}{n} \sum_{i=1}^{n} e \times 100\%, e_{\rm R} = \frac{1}{n} \sum_{i=1}^{n} |e| \times 100\%, e_{\rm S} = \sqrt{\frac{1}{n} \sum_{i=1}^{n} e^2} \times 100\%$$
 (21)

Where  $e_A$  is the average relative error,  $e_R$  is the average absolute relative error, and  $e_S$  is the root mean square error.

#### 3.3. Analysis of internal forces in fluids

In recent years, the concept of supercritical boiling has been widely studied, and this phenomenon was detected macroscopically by Maxim et al. [41] using neutron imaging technology in 2019. The phase changes of water molecules under supercritical pressure, resembling liquid and gas, have been confirmed. Recently, He et al. [42,43] was the first to directly observe evaporative and boiling heat transfer at multiple scales through fiber optic measurement methods, and quantitatively characterized the proportion of boiling like heat transfer in the total heat transfer rate through experiments, fully considering the influence of two-phase flow patterns on heat transfer modes. Dong et al. [44] used molecular dynamics (MD) to observe the nucleation position of bubbles and the formation of stable pseudo films under supercritical conditions, and defined the initial nucleate boiling point (ONB point) under supercritical conditions based on the competitive relationship between kinetic energy and potential energy. Banuti [32] first proposed to define the phase classification of fluids under supercritical pressure based on the specific heat capacity of the fluid, using the step phenomenon of physical properties before and after boiling in a quasi Biya critical state as a reference. Fig. 12(a) shows the phase distribution of CO2 under subcritical and supercritical conditions,  $\Delta i_{pc}$  represents the enthalpy change required for the transition between gas and liquid phases, manifested as intrinsic latent heat in subcritical conditions and additional sensible heat required to maintain the phase transition in supercritical conditions. Its specific definition is as follows [22]:

$$\Delta i_{pc} = \int_{T}^{T^{+}} c_{P} dT = i(T^{+}) - i(T^{-})$$
 (22)

Where  $\Delta i_{pc}$  is the enthalpy of quasi phase transition of fluids under supercritical pressure,  $T^+$  and  $T^-$  are the temperatures of the supercritical fluid in the gaseous and liquid states, respectively;  $c_P$  is the specific heat capacity at constant pressure.

As shown in Fig. 12(c), there are four types of forces acting on the boiling flow process of  $sCO_2$ , namely inertial force  $(F_I)$ , viscous force  $(F_V)$ , evaporative momentum force  $(F_M)$ , and buoyancy force  $(F_R)$ . The  $F_I$  is highly correlated with the velocity of the fluid, and its radial distribution is subject to the influence of the shear force  $(F_V + F_R)$ . When  $F_R$  starts to emerge, the velocity profile deforms accordingly. Instead of reaching its maximum value at the central axis of the pipe, the  $F_I$  moves closer to the wall surface. When  $F_R$  is equal in magnitude and opposite in direction to  $F_V$ , a maximum  $F_I$  appears near the wall, similar to an M-type  $F_I$  curve distribution. As the M-type  $F_I$  curve develops, the shear force decreases to zero, and even the direction may reverse, as shown in the radial distribution of shear force from 1 to 2 in Fig. 12(c). According to the definition of  $F_M$  proposed by Kandlikar [45], this article believes that  $F_M$  is caused by the evaporation and expansion of the gas like film

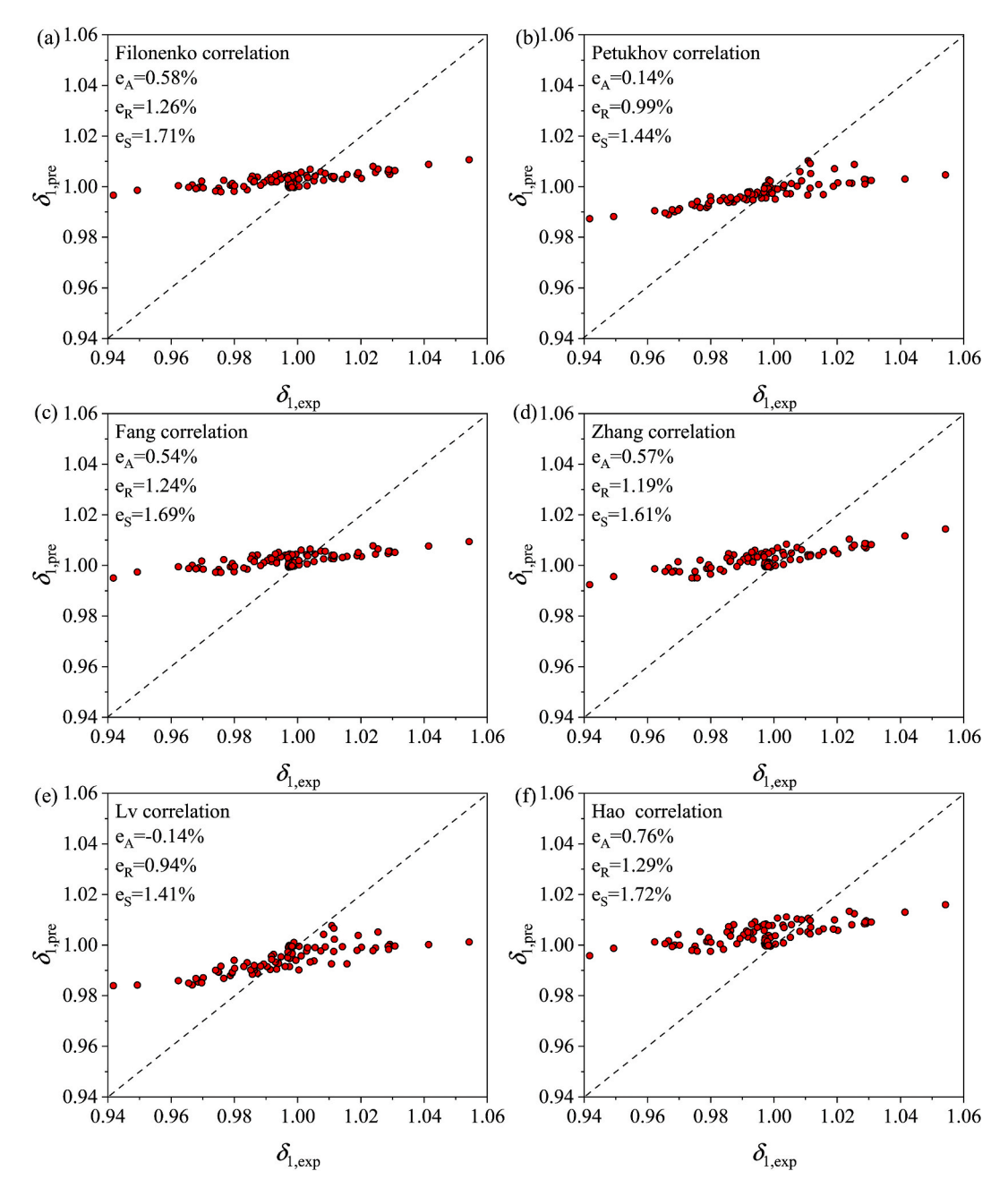


Fig. 11. Comparison of various correlation prediction values of traffic allocation ratio with actual experimental values.

layer near the wall. Therefore, the occurrence location of  $F_{\rm M}$  is set at the contact surface between the two phases determined by  $T^+$ . Based on the above argument of supercritical boiling theory, this paper introduces dimensionless numbers such as K, Re, Bu, which are commonly used to analyze subcritical fluid flow and heat transfer, into the analysis of internal forces in sCO<sub>2</sub>. The specific definitions are as follows [30,46]:

$$K = \frac{F_{\rm M}}{F_{\rm I}} = \frac{1}{m} \sum_{1}^{m} \left( \frac{q_{\rm w}}{Gi_{\rm w}(z)} \right)^{2} \frac{\rho_{\rm LL}(z)}{\rho_{\rm VL}(z)}, m = 40$$
 (23)

$$Re_{\rm b} = \frac{F_{\rm I}}{F_{\rm V}} = \frac{1}{m} \sum_{1}^{m} \frac{Gd_{\rm i}}{\eta(z)}$$
 (24)

$$Bu = \frac{F_{R}}{F_{I}} = \frac{Gr}{Re^{2}} = \frac{\mathrm{gd_{i}}\rho_{\mathrm{b,ave}}(\rho_{\mathrm{b,in}} - \rho_{\mathrm{b,ave}})}{G^{2}}$$
(25)

Where *K* represents the accumulation of the thickness of the quasi gas

film during boiling heat transfer, and is the ratio of the evaporation momentum force on the bubble to the inertia force; Re is the ratio of fluid inertial force to viscous force, Bu is the ratio of buoyancy force to inertial force acting on the fluid, m is the number of sections of the experimental pipeline that have been divided,  $i_w(z)$  is the fluid enthalpy at the local mainstream temperature,  $\rho_{\rm LL}(z)$  is the local fluid density at the inner wall temperature of the pipeline, and  $\rho_{\rm LL}(z)$  is the estimated local fluid density at the outer wall temperature of the pipeline.

Fig.13 analyzes the relationship between these dimensionless numbers and pressure drop, and finds that frictional pressure drop is directly proportional to K and Re, while gravitational pressure drop is partially inversely proportional to Bu and Re. In contrast, there is a mutually reinforcing relationship between K and Re. In a parallel tube group, when the strong heated tube accumulates a gas like film layer due to boiling heat transfer, it often exacerbates the turbulent flow in the single tube. This is consistent with the conclusion in Ref. [21] that the decrease in working fluid density in high heat flux tubes in a parallel

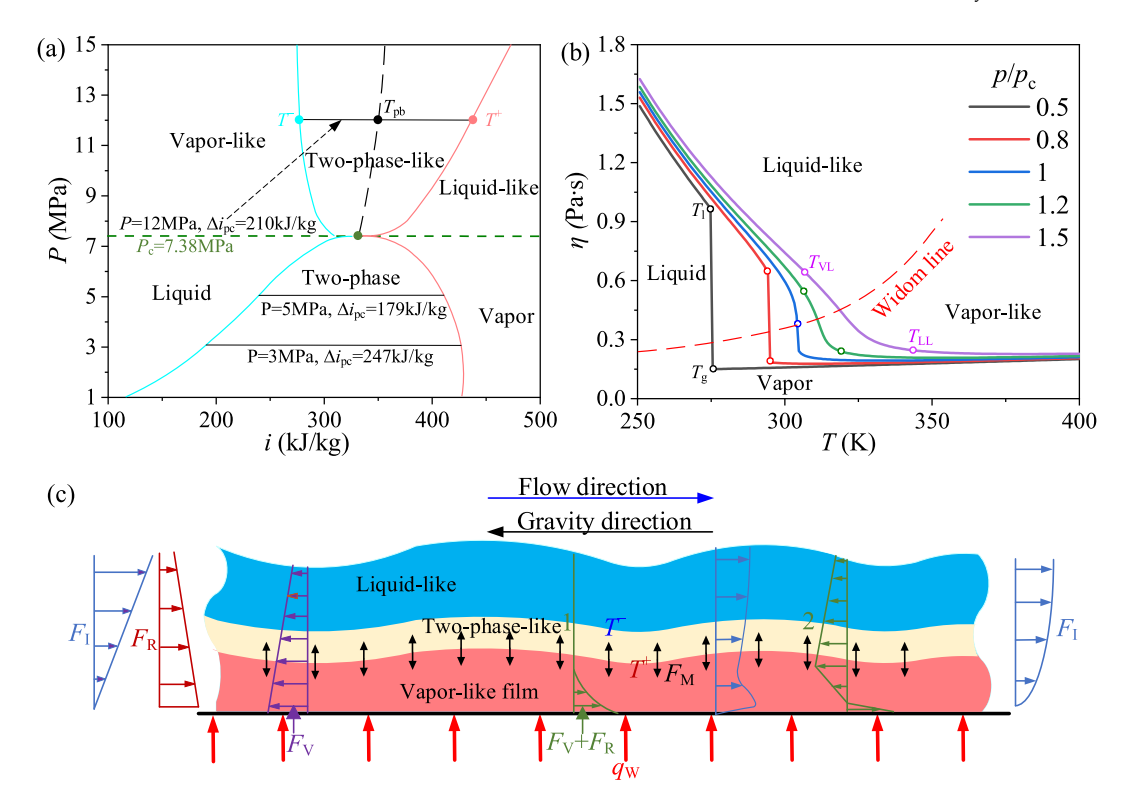


Fig. 12. Thermodynamic characteristics of CO<sub>2</sub> and analysis of flow forces inside pipes(a: phase distribution, b: Viscosity characteristics, c: analysis of forces).

tube group leads to an increase in volumetric flow velocity. There is a clear competitive relationship between Bu and Re. When the gravity pressure drop reaches its maximum value, both Bu and Re reach their minimum values. However, when the gravity pressure drop reaches its minimum value, Bu and Re may not be able to maintain their minimum values. The enhancement of turbulence inside the tube will intensify the mixing of cold and hot fluids, thereby reducing the temperature gradient inside the tube. This is also the reason why the inertial force in forced convection will significantly weaken the buoyancy force in flow heat transfer.

Taking inspiration from Figs. 11 and 13, due to the pressure drop analysis in parallel pipelines can confirm the flow distribution relationship, and the fluid stress inside the pipeline can fully reflect the pressure drop changes inside the pipeline, whether the force analysis angle accurately can predict the flow distribution between pipelines?

Please refer to the following text. As shown in Fig. 14, the heat transfer process in parallel tubes is classified into the following three types based on the relative magnitude of gravitational and frictional pressure drops between tubes (the difference in acceleration pressure drop between tubes is almost zero, see Fig. 9). It is as follows:

The first type is where the difference in gravitational pressure drop between tubes is greater than the difference in frictional pressure drop. The pipe with higher heat flux has less internal flow resistance, and the heat deviation causes the high-density region of the pseudo-liquid in the strongly heated pipe to become smaller along the flow direction, resulting in a lower viscosity and greater density difference. Shear force plays a dominant role, among which a sudden decrease in viscous force and an increase in buoyancy force can cause pipelines with high heat flux density to attract more flow, so the flow distribution presents as an SCC state, typically occurring under normal heat transfer (NHT)

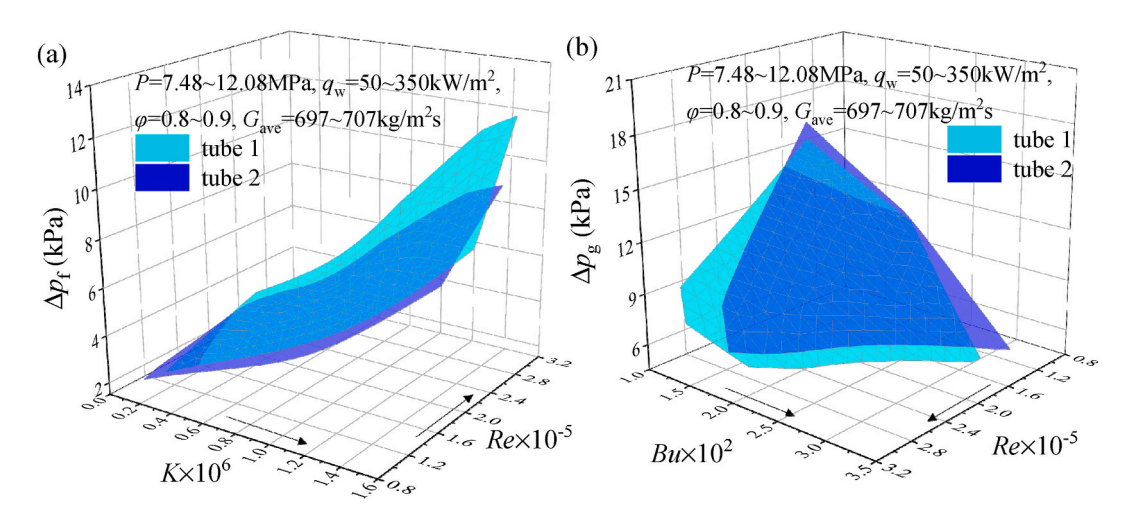
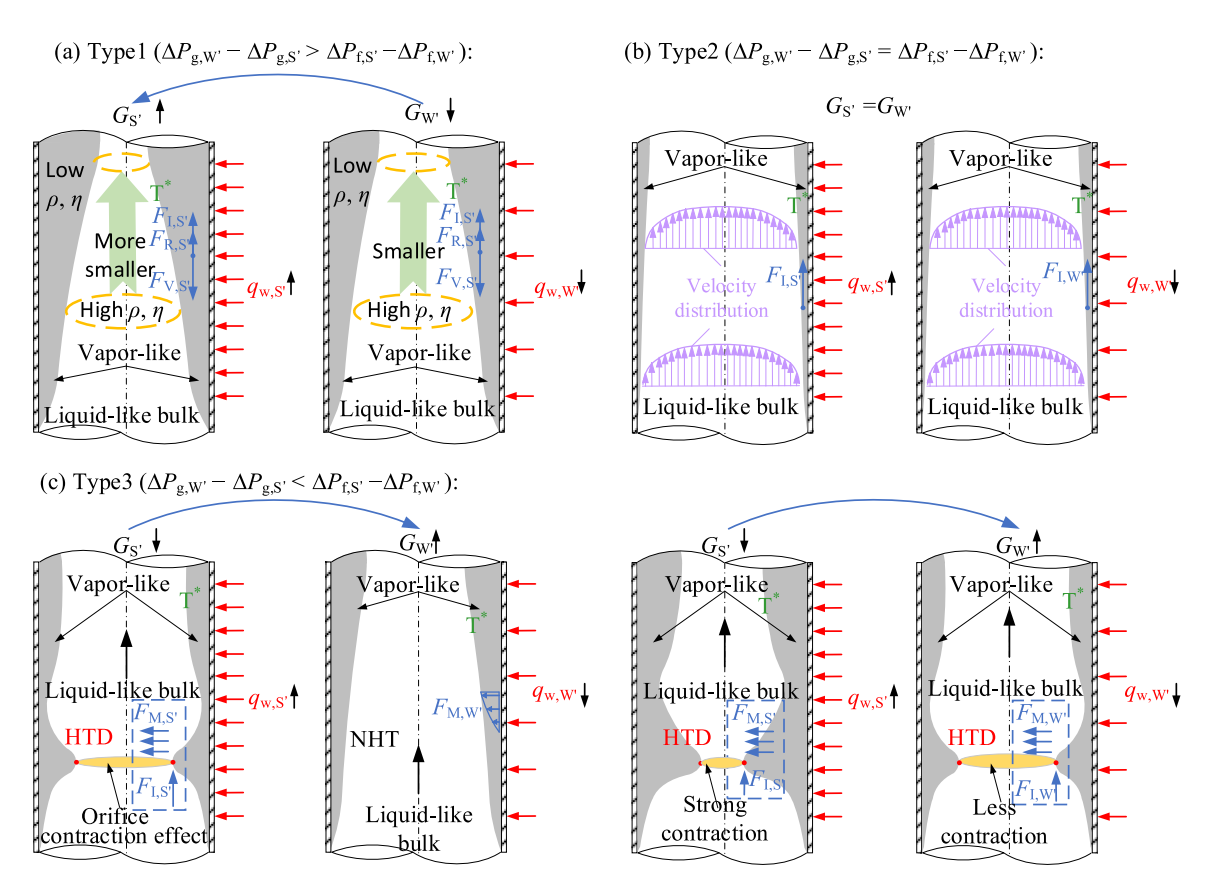


Fig. 13. The relationship between dimensionless numbers and pressure drop (a: Effect of K, Re on friction pressure drops, b: Effect of Bu, Re on gravity pressure drops).



**Fig. 14.** Mechanism analysis of flow deviation caused by thermal deviation (indicated by the subscript below: S' represents strong heating, W' represents weak heating) [11,35,47,48].

conditions with low mass flow rates. The second type is where the difference in gravitational pressure drop between tubes is almost equal to the difference in frictional pressure drop. The flow resistance inside the tubes remains almost unchanged before and after the heat deviation, and under the maintenance of strong inertial force  $F_{\rm I}$ , the velocity distribution along the tube length changes little. Thus, the flow presents a uniform distribution, generally occurring under conditions of high mass flow rates with low heat flux. The third type is where the difference in gravitational pressure drop between tubes is less than the difference in frictional pressure drop. The stronger the heating, the greater the internal flow resistance in the tube. The heat deviation causes the thickness of the vapor-film-like to accumulate in the strongly heated tube, reducing the flow area of the LL mainstream (OCE occurs). Under the dominance of the vapor momentum force  $F_{\rm M}$ , more flow is pushed towards the weakly heated tube, so the flow distribution presents as an inverse SCC state, typically occurring during heat transfer deterioration (HTD) in single or multiple tubes.

In summary, from the perspective of force analysis, analyzing the competition between steam momentum force and shear force (the combined force of buoyancy and viscosity) relative to inertial force can predict flow distribution. The type of flow distribution in the parallel tubes is distinguished based on the heat flux density value when the total pressure drops of tubes 1 and 2 in the testing loop shown in Fig. 9(a) are equal, as presented in Fig. 15. As the heat flux density increases, the flow and heat transfer situation gradually transitions from Type 1 to Type 2 and then to Type 3. When  $\frac{Re_1}{Re_2} > 1.06$ , both the near neighbor boundary and the far critical boundary are dominated by viscous or buoyant forces. The low viscosity of high-temperature fluids can even cause a decrease in frictional pressure drop (see Fig. 9(a)), and the flow distribution state is in Type 1; Only when the momentum force and shear force of evaporation inside the tube reach equilibrium, the inertial force

dominates the flow distribution state and is in Type 2; When  $\frac{K_1}{K_2} > 1.2 \& \frac{Re_1}{Re_2} < 1.06$ , evaporative momentum force dominates, resulting in a Type 3 flow distribution. Meanwhile, when  $\frac{q_w}{G} > 0.36$ , the changes in  $\frac{K_1}{K_2}$  and  $\frac{Bu_1}{Bu_2}$  are relatively smooth, indicating a threshold in the impact of heat deviation on uneven flow distribution. Additionally, the peak value of a can accurately predict the critical  $q_w$  at which heat transfer deterioration occurs in high heat flux density tube 1, but its changing trend cannot reflect the direction of flow distribution ratio, which is inseparable from the weakening of buoyancy force by inertial force in forced convection.

Finally, Fig. 15 inspired us to establish a correlation equation in the form of  $\frac{G_1}{G_2}=a_1\left(\frac{K_1}{K_2}\right)^{a_2}\left(\frac{Bu_1}{Bu_2}\right)^{a_3}\left(\frac{Re_1}{Re_2}\right)^{a_4}$ , where  $a_1,\,a_2,\,a_3$ , and  $a_4$  are the corresponding coefficients obtained by taking the logarithm of the original formula and then using the principle of the linear regression. The new equation for the flow distribution ratio  $\delta_1$  is obtained as follows:

$$\delta_1 = \frac{2\varpi}{1+\varpi}, \varpi = \frac{G_1}{G_2} = 0.9978 \left(\frac{K_1}{K_2}\right)^{-0.2229} \left(\frac{Bu_1}{Bu_2}\right)^{0.022} \left(\frac{Re_1}{Re_2}\right)^{0.8486}$$
 (26)

Where  $\omega$  is the ratio of mass flow velocity between heating testing loop tubes 1 and 2.

Fig. 16 shows the comparison between the new correlation and experimental results The errors of  $e_A$ ,  $e_R$  and  $e_S$  are -0.04%, 0.73%, and 0.90%, respectively, indicating a significant improvement in prediction accuracy.

# 4. Conclusions

This paper experimentally investigates the flow distribution char-

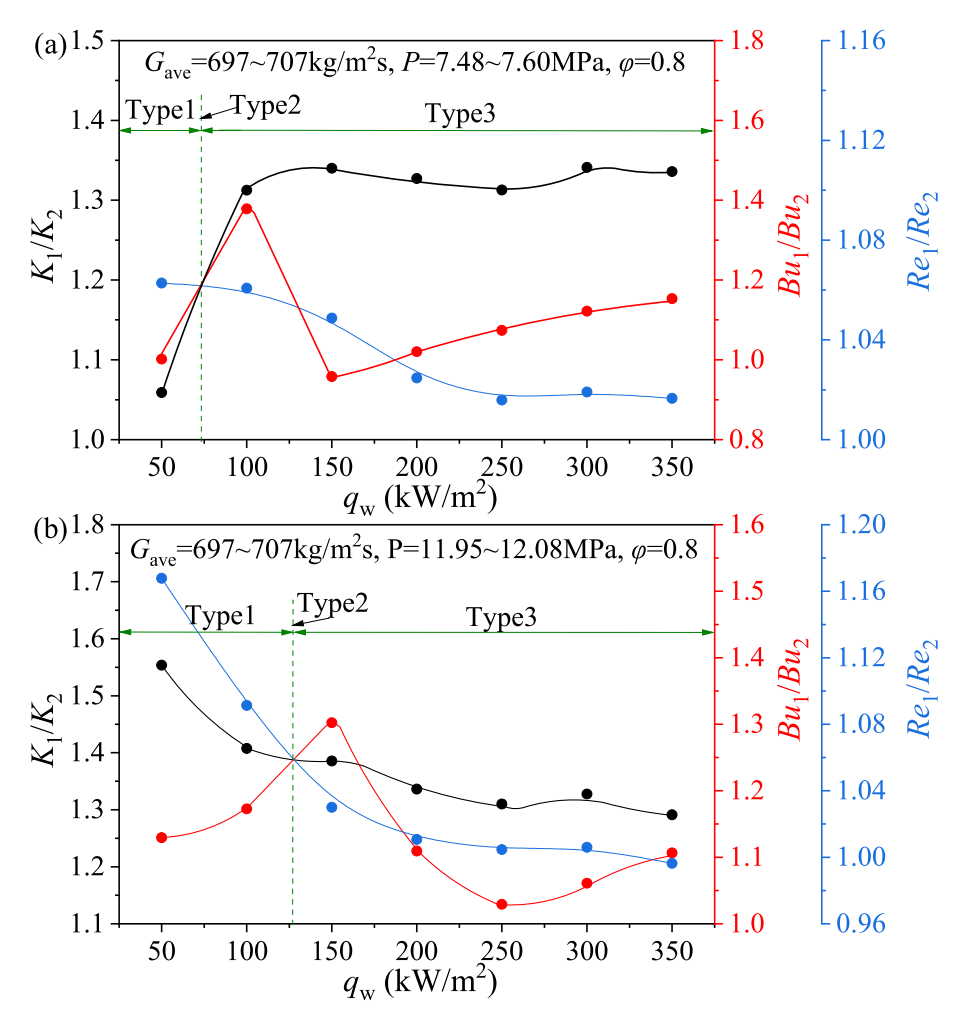


Fig. 15. Transition situation of flow distribution types in parallel pipes.

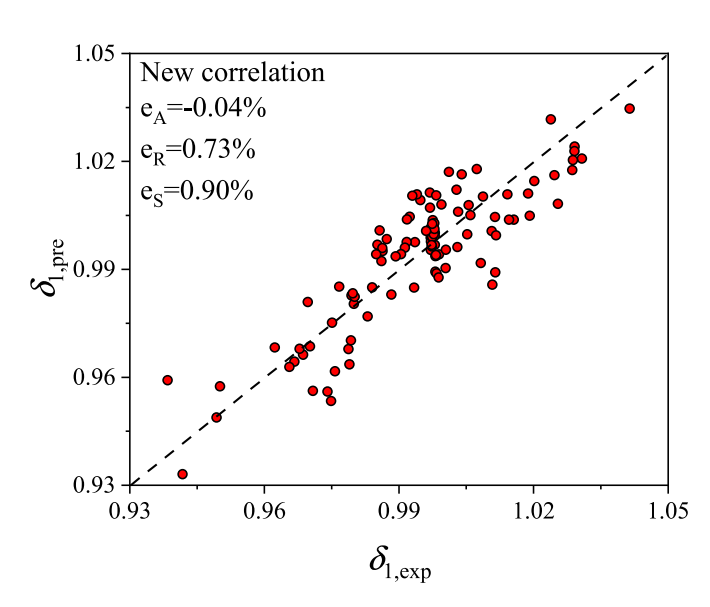


Fig. 16. Prediction results of experimental correlations.

acteristics of sCO $_2$  flowing upwards in vertical parallel pipes. The study examines the effects of mass flux, heat flux density, working pressure, and thermal deviation on flow distribution characteristics, with the parameters set at 7.5 MPa $\sim$ 15 MPa, 600 kg/m $^2$ s $\sim$ 1400 kg/m $^2$ s, 50 kW/m $^2$ ~350 kW/m $^2$  and 0.8 $\sim$ 1.25, respectively. The research results can be

applied to the start stop process of  $sCO_2$  Rankine cycle heat exchange system or  $sCO_2$  Brayton cycle heat exchange system. The main conclusions are as follows.

- 1. When heating  $\mathrm{CO}_2$  in vertical parallel pipes with an inner diameter of 10 mm, the heat shift between the tubes does not necessarily cause a flow shift. Under normal heat transfer conditions, lower mass flow rates enhance the SCC, making the strongly heated tube more likely to attract more flow. Under deteriorated heat transfer conditions, vapor-film-like film expansion hinders the main flow, and the resulting OCE causes the weakly heated tube to attract more flow, with the degree of reverse SCC becoming stronger as the mass flow rate decreases. Additionally, increasing pressure enhances SCC while weakening the effect of OCE, promoting uniform flow distribution and helping maintain the balance of wall temperatures between the tubes.
- 2. An experimental relationship in the form of  $\frac{G_1}{G_2} = a_1 \left(\frac{K_1}{K_2}\right)^{a_2} \left(\frac{Bu_1}{Bu_2}\right)^{a_3} \left(\frac{Re_1}{Re_2}\right)^{a_4}$  is proposed, suggesting that evaporative momentum force, shear force, and inertial force collectively determine the trend of flow distribution changes. Therefore, when the mass flow rate of  $CO_2$  in the vertical tube group is low, the shear force dominates, and strong heat exchange causes a higher density difference along the flow direction, making the flow more likely to present an SCC distribution. The sharp changes in fluid thermal properties  $\alpha_V$  and  $\eta$  during heat transfer across large specific heat

- capacity regions can lead to changes in the direction of shear forces, which is the reason for SCC fluctuations. When the degree of heat unevenness reaches a threshold, even if the heat difference continues to increase, the interaction force between the tubes will not change, indicating a limit to the impact of thermal deviation on flow distribution.
- 3. During the start-up and shutdown process of the boiler, attention should be paid to applying high heat load or high heat load change rate while ensuring sufficient fluid circulation in the pipes. This effectively avoids uneven flow caused by uneven heat, and thus avoids safety accidents such as wall temperature overshoot of water-cooled wall pipelines. At the same time, this study suggests that the critical SBO number required to ensure the existence of SCC phenomenon within the pressure range of 7.5 MPa $\sim$ 15 MPa varies nonlinearly. When the system pressure satisfies  $P > \frac{15.1-60241.0SBO}{1-4016.1SBO}$ , synchronously increasing the thermal load of the boiler water-cooled wall during the start-up process has a certain safety guarantee. The self compensation characteristic of the riser group can slow down the occurrence of HTD phenomenon.
- 4. Compared with the flow distribution model established from the perspective of pressure drop analysis, the new correlation equation has improved prediction accuracy, providing theoretical guidance and assistance for the design and operation of sCO<sub>2</sub> boilers.

#### Nomenclature

$a_1, a_2,$	constants	ave	average
$a_{3,}$			
$a_4$			
a	ratio of inner and outer	cr	critical point
	diameters of the experimental		
	section pipeline		
Bu	buoyancy parameter	exp	experimental
d	tube diameter, m	f	friction
e	error	I	inertia
F	Force, N	i	internal
f	friction factor	in	inlet
Gr	Grashof number	LL	liquid-like
K	non-dimensional number	M	evaporation momentum
L	axial length of experimental	0	outside
	section pipeline		
1	rectangular hole side length	out	outlet
G	mass flow rate, kg/m <sup>2</sup> s	pre	predictive
g	gravitational acceleration, with	R'	buoyancy
	a value of 9.8 m/s <sup>2</sup>		
ṁ	mass flow, kg/s	R	mean absolute relative
P	pressure, MPa	S'	strong heating
$P_{\rm c}$	heating power of single tube, kW	S	root-mean-square relative
q	heat flux, kW/m <sup>2</sup>	t	total
Re	Reynolds number	VL	vapor-like
r	radial distance between the	W'	weak heating
	fluid element and the center of		
	the circle in the current section,		
	m		
$sCO_2$	supercritical carbon dioxide	w	wall
SCC	self compensation	Greek	symbols
	characteristics		
SBO	supercritical boiling number	$\Delta H$	height difference between the
			upper and lower parts of the
			testing loop pipeline, m
OCE	orifice throttling effect	$\Delta P$	pressure drop, kPa
$T^*$	termination of pseudo-boiling	$\Delta P_{ m g}$	gravitational pressure drop,
	temperature		kPa
T	temperature	$\Delta P_{ m L}$	local pressure drop, kPa
и	flow velocity of the fluid	$\Delta P_{\mathrm{t}}$	pressure drop measured by the
	element along the length		differential pressure
	direction of the pipe, m/s		transmitter in the heating
			testing loop, kPa
			(continued on next column)

#### (continued)

the outlet dryness of	$\alpha_{v}$	volume expansion coefficient,/
-	•••	K
axial coordinates, m	λ	thermal conductivity, W/m·K
pts	$\theta$	angle between the testing loop
		pipeline and the horizontal
		line, with a value of 90°
pipeline number	$\varphi$	thermal deviation
mean relative	δ	flow distribution ratio
accelerated	ρ	density, kg/m <sup>3</sup>
arterial road	η	dynamic viscosity, Pa·s
mainstream	$\overline{w}$	ratio of inter-tube mass flow
		rate
	pipeline number mean relative accelerated arterial road	experimental section pipeline axial coordinates, m $\lambda$ pts $\theta$ pipeline number $\phi$ mean relative $\delta$ accelerated $\rho$ arterial road $\eta$

## CRediT authorship contribution statement

**Wenxuan Cao:** Investigation, Data curation. **Jinliang Xu:** Writing – review & editing, Methodology. **Enhui Sun:** Visualization, Methodology. **Yaru Ma:** Writing – review & editing.

#### Declaration of competing interest

We state that the manuscript titled "Experimental investigation on the uneven distribution characteristics of  $sCO_2$  flow in vertically parallel double pipes with non-uniform heating" by Wenxuan Cao, Jinliang Xu, Enhui Sun, Yaru Ma does not have any conflict of interest including any financial, personal, or other relationships with other people or organizations.

# Acknowledgements

This study has been supported by the National Key R&D Program of China (No. 2023YFB4102202), and the National Natural Science Foundation of China (No. 52130608), and the National Natural Science Foundation of China (No. 52206010).

# Data availability

Data will be made available on request.

#### References

- D. Yang, G. Tang, K. Luo, et al., Integration and conversion of supercritical carbon dioxide coal-fired power cycle and high-efficiency energy storage cycle: feasibility analysis based on a three-step strategy, Energy Convers. Manag. 269 (2022) 116074.
- [2] E. Sun, J. Xu, M. Li, et al., Connected-top-bottom-cycle to cascade utilize flue gas heat for supercritical carbon dioxide coal fired power plant, Energy Convers. Manag. 172 (2018) 138–154.
- [3] D. Wang, Y. Zhou, L. Si, et al., Performance study of 660 MW coal-fired power plant coupled transcritical carbon dioxide energy storage cycle: sensitivity and dynamic characteristic analysis, Energy 293 (2024) 130663.
- [4] M. Khoshvaght-Aliabadi, P. Ghodrati, M. Salami, et al., Turbulent supercritical CO<sub>2</sub> flow and cooling heat transfer in vertical alternating flattened tubes, Int. Commun. Heat Mass Tran. 162 (2025) 108565.
- [5] Ghodrati Parvaneh, Morteza Khoshvaght-Aliabadi, Supercritical CO<sub>2</sub> flow and heat transfer through tapered horizontal mini-tubes: parametric analysis and optimization study, Appl. Therm. Eng. 242 (2024) 122512.
- [6] Shuoshuo Li, Xinxin Liu, Yu Zeng, et al., Numerical study of dimpled structures on heat transfer deterioration mitigation with supercritical CO<sub>2</sub> heated in vertical tube, Appl. Therm. Eng. 259 (2025) 124925.
- [7] X.L. Li, X.Y. Yu, P.T. Liu, et al., S-CO<sub>2</sub> flow in vertical tubes of large-diameter: experimental evaluation and numerical exploration for heat transfer deterioration and prevention. Int. J. Heat Mass Tran. 216 (2023) 124563.
- [8] L. Chai, S.A. Tassou, Recent progress on high temperature and high pressure heat exchangers for supercritical CO<sub>2</sub> power generation and conversion systems, Heat Transf. Eng. 44 (21–22) (2023) 1950–1968.
- [9] C. Liu, Z. Miao, J. Xu, et al., Novel matching strategy for the coupling of heat flux in furnace side and CO<sub>2</sub> temperature in tube side to control the cooling wall temperatures, J. Therm. Sci. 30 (4) (2021) 1251–1267.
- [10] Q. Wang, J. Xu, C. Zhang, et al., A critical review on heat transfer of supercritical fluids, Heat Transf. Eng. 44 (21–22) (2023) 1969–1994.
- [11] C. Liu, J. Xu, M. Li, et al., Scale law of sCO<sub>2</sub> coal fired power plants regarding system performance dependent on power capacities, Energy Convers. Manag. 226 (2020) 113505.

- [12] M.M. Ehsan, M. Awais, S. Lee, et al., Potential prospects of supercritical CO<sub>2</sub> power cycles for commercialisation: applicability, research status, and advancement, Renew. Sustain. Energy Rev. 172 (2023) 113044.
- [13] Z. Wang, J. Xu, T. Wang, et al., Performance of sCO<sub>2</sub> coal-fired power plants at various power capacities, J. Clean. Prod. 416 (2023) 137949.
- [14] J. Zhou, D. Huang, Y. Qi, Modeling and thermodynamic analysis of gassupercritical carbon dioxide combined cycle system, Energy Sources, Part A Recovery, Util. Environ. Eff. 44 (4) (2022) 9043–9063.
- [15] J. Xu, E. Sun, M. Li, et al., Key issues and solution strategies for supercritical carbon dioxide coal fired power plant, Energy 157 (2018) 227–246.
- [16] E.H. Sun, H. Hu, H. Li, et al., How to construct a combined S-CO<sub>2</sub> cycle for coal fired power plant? Entropy 21 (1) (2019) 19.
- [17] Y. Xi, W. Kai, Z. Chao, et al., Efficiency improvement technology of front and rear wall hedging boilers based on combustion optimization and balancing heating surface wall temperature, Energy Rep. 8 (2022) 383–391.
- [18] X. Zhu, Q. Bi, Q. Su, et al., Self-compensating characteristic of steam-water mixture at low mass velocity in vertical upward parallel internally ribbed tubes, Appl. Therm. Eng. 30 (16) (2010) 2370–2377.
- [19] K. Kurose, K. Miyata, Y. Hamamoto, et al., Flow boiling heat transfer and flow distribution of HFC32 and HFC134a in unequally heated parallel mini-channels, Int. J. Refrig. 119 (2020) 305–315.
- [20] A. Miglani, A. Soto, J.A. Weibel, et al., The effect of uneven heating on the flow distribution between parallel microchannels undergoing boiling, J. Electron. Packag. 143 (4) (2021) 041107.
- [21] S. Zheng, P. Guo, J. Yan, et al., Experimental investigation of the flow distribution of high-pressure CO<sub>2</sub> flowing in heated parallel channels, J. Supercrit. Fluids 184 (2022) 105569.
- [22] Q. Wang, X. Ma, J. Xu, et al., The three-regime-model for pseudo-boiling in supercritical pressure, Int. J. Heat Mass Tran. 181 (2021) 121875.
- [23] N.P. Longmire, S.L. Showalter, D.T. Banuti, Holding water in a sieve-stable droplets without surface tension, Nat. Commun. 14 (1) (2023) 3983.
- [24] H. Zhang, J. Xu, X. Zhu, Dimensional analysis of flow and heat transfer of supercritical CO<sub>2</sub> based on pseudo-boiling theory, Acta Phys. Sin. 70 (4) (2021) 044401
- [25] X. Wang, J. Cai, Z. Lin, et al., Dynamic simulation study of the start-up and shutdown processes for a recompression CO<sub>2</sub> Brayton cycle, Energy 259 (2022) 124028
- [26] J. Taler, W. Zima, P. Ocłoń, et al., Mathematical model of a supercritical power boiler for simulating rapid changes in boiler thermal loading, Energy 175 (2019) 500 500
- [27] Cui X, Wang Y, Yang J, Li Y, et al. Performance analysis and multi-objective optimization of CO<sub>2</sub> transcritical Rankine cycle systems driven by solar energy. Sol. Energy. 286: 113179.
- [28] X. Feng, F. Shi, G. Qiao, et al., Integrating organic Rankine cycle with thermoelectric generator in various applications utilizing low-grade energy: a review, Sustain. Energy Technol. Assessments 68 (2024) 103882.

- [29] B. Zhu, J. Xu, X. Wu, et al., Supercritical "boiling" number, a new parameter to distinguish two regimes of carbon dioxide heat transfer in tubes, Int. J. Therm. Sci. 136 (2019) 254–266.
- [30] H. Zhang, J. Xu, X. Zhu, et al., The K number, a new analogy criterion number to connect pressure drop and heat transfer of sCO<sub>2</sub> in vertical tubes, Appl. Therm. Eng. 182 (2021) 116078.
- [31] C. Liu, J. Xu, M. Li, et al., The comprehensive solution to decrease cooling wall temperatures of sCO<sub>2</sub> boiler for coal fired power plant, Energy 252 (2022) 124021.
- [32] D.T. Banuti, Crossing the widom-line-supercritical pseudo-boiling, J. Supercrit. Fluids 98 (2015) 12–16.
- [33] J. Liu, H. Li, X. Lei, et al., An improved model on flow distributions of supercritical pressure water in parallel heated pipes, Appl. Therm. Eng. 130 (2018) 793–803.
- [34] Y. Zou, P.S. Hrnjak, Single-phase and two-phase flow pressure drop in the vertical header of microchannel heat exchanger, Int. J. Refrig. 44 (2014) 12–22.
- [35] P. Yang, W. Ling, K. Tian, et al., Flow distribution and heat transfer performance of two-phase flow in parallel flow heat exchange system, Energy 270 (2023) 126957.
- [36] G.K. Filonenko, Hydraulic resistance of pipelines, Therm. Eng. (4) (1954) 40-44.
- [37] B.S. Petukhov, V.A. Kurganov, V.B. Ankudinov, Heat transfer and flow resistance in the turbulent pipe flow of a fluid with near-critical state parameters, Teplofiz. Vysok. Temp. 21 (1983) 92–100.
- [38] X. Fang, L. Xu, Y. Chen, et al., Correlations for friction factor of turbulent pipe flow under supercritical pressure: review and a new correlation, Prog. Nucl. Energy 118 (2020) 103085.
- [39] H. Lyu, H. Wang, Q. Bi, F. Niu, Experimental investigation on heat transfer and pressure drop of supercritical carbon dioxide in a mini vertical upward flow, Energies 15 (17) (2022) 6135.
- [40] B. Hao, C. Zhang, L. Cheng, et al., Experimental investigation on the pressure drop characteristics of subcritical and supercritical CO<sub>2</sub> heated in a horizontal tube, Int. J. Heat Mass Tran. 201 (2023) 123650.
- [41] F. Maxim, C. Contescu, P. Boillat, et al., Visualization of supercritical water pseudoboiling at Widom line crossover, Nat. Commun. 10 (1) (2019) 4114.
- [42] X. He, J. Xu, X. Yu, et al., Distinguishing evaporation-like and boiling-like modes of pseudo-boiling in supercritical pressures, Int. J. Heat Mass Tran. 214 (2023) 124417
- [43] X. He, J. Xu, J. Xie, Quantitative characterization of the pseudo-boiling contribution to supercritical heat transfer, Phys. Fluids 36 (1) (2024) 1070–6631.
- [44] M. Dong, J. Xu, Y. Wang, Critical threshold for bubble-like nucleation during pseudoboiling at supercritical pressures, Langmuir (2024) 743–7463.
- [45] S.G. Kandlikar, Heat transfer mechanisms during flow boiling in microchannels, Heat Transfer 126 (1) (2004) 8–16.
- [46] B. Shiralkar, P. Griffith, The effect of swirl, inlet conditions, flow direction, and tube diameter on the heat transfer to fluids at supercritical pressure, J. Heat Tran. 92 (3) (1970) 465–471.
- [47] L. Cheng, J. Xu, W. Cao, et al., Supercritical carbon dioxide heat transfer in horizontal tube based on the Froude number analysis, Energy 294 (2024) 130980.
- [48] D. Cai, X. Xu, S. Zhang, et al., Experimental investigation on the flow instability of supercritical CO<sub>2</sub> in vertical upward circular tube in transcritical CO<sub>2</sub> Rankine system, Appl. Therm. Eng. 183 (2021) 116139.